

Detecting quantum entanglement with unsupervised learning

Yiwei Chen,¹ Yu Pan,^{1,*} Guofeng Zhang,^{2,†} and Shuming Cheng^{3,4,5,‡}

¹*Institute of Cyber-Systems and Control, College of Control Science and Engineering, Zhejiang University, Hangzhou, 310027, China*

²*Department of Applied Mathematics, The Hong Kong Polytechnic University, Hung Hom, Kowloon, Hong Kong*

³*The Department of Control Science and Engineering, Tongji University, Shanghai 201804, China*

⁴*Shanghai Institute of Intelligent Science and Technology, Tongji University, Shanghai 201804, China*

⁵*Institute for Advanced Study, Tongji University, Shanghai, 200092, China*

(Dated: March 9, 2021)

Quantum properties, such as entanglement and coherence, are indispensable resources in various quantum information processing tasks. However, there still lacks an efficient and scalable way to detecting these useful features especially for high-dimensional quantum systems. In this work, we exploit the convexity of normal samples without quantum features and design an unsupervised machine learning method to detect the presence of quantum features as anomalies. Particularly, given the task of entanglement detection, we propose a complex-valued neural network composed of pseudo-siamese network and generative adversarial net, and then train it with only separable states to construct non-linear witnesses for entanglement. It is shown via numerical examples, ranging from 2-qubit to 10-qubit systems, that our network is able to achieve high detection accuracy with above 97.5% on average. Moreover, it is capable of revealing rich structures of entanglement, such as partial entanglement among subsystems. Our results are readily applicable to the detection of other quantum resources such as Bell nonlocality and steerability, indicating that our work could provide a powerful tool to extract quantum features hidden in high-dimensional quantum data.

PACS numbers:

I. INTRODUCTION

Peculiar quantum features, signalled by quantum entanglement [1] and coherence [2], enable us to accomplish tasks impossible for classical systems [3], such as ensuring the security of communications and speeding up certain hard computational tasks [4, 5]. Hence, an important question naturally arises: How can the presence of these features be efficiently detected for any given quantum system? Indeed, this is a challenging task for high-dimensional systems because quantum features usually imply some correlated patterns hidden within subsystems. Taking entanglement for example, except for low-dimensional systems, e.g., $2 \otimes 2$ and $2 \otimes 3$, of which entanglement could be detected faithfully via the Positive Partial Transpose (PPT) criterion [6], generically, it is an NP-hard problem [7]. Besides, even though at least one linear entanglement witness could be found to witness any entangled state [1, 8–10] as displayed in Fig. 1, there still lacks a universal and scalable way to construct such an appropriate witness for an arbitrary state in practice.

In this work, we turn to the machine learning technique which is powerful in extracting features or patterns hidden in large high-dimensional datasets to tackle the quantum detection problem. Recently, much progress has been achieved in this inter-disciplinary field of quantum machine learning [11]. For example, on one hand, many

quantum or quantum-inspired algorithms have been developed to speed up some well-known machine learning algorithms [12–14]. On the other hand, machine learning is also a natural candidate to extract correlated features of high-dimensional quantum systems, which has found wide applications in quantum control [15], state tomography [16], measurement [17, 18], and many-body problems [19–21]. Especially, the task of quantum entanglement detection could be formulated as a binary classification problem. As a consequence, various classical neural nets, trained with both entangled and separable samples, have been constructed to solve this problem via supervised learning [22–24]. However, the supervised training method requires a large pre-labelled dataset. In practice, it is time-consuming or even impossible to faithfully label a large number of entangled states in a high-dimensional space [7], thus leading these supervised methods into a dilemma.

By exploiting the fact that entangled samples are distinguishable from the convex set of all separable states, we instead build up an unsupervised model to accomplish such a detection task beyond the above issues. Indeed, it becomes an anomaly detection problem of which all separable samples are labelled as normal. As shown in Fig. 2, a class of complex-valued neural networks, composed of a pseudo-siamese network and a Generative Adversarial Net (GAN), is constructed and then trained with very few normal samples to detect entanglement for high-dimensional systems, ranging from 2-qubit to 10-qubit states. It is noted that our model is much more feasible than anomaly detection methods proposed in [25, 26] which require quantum nets.

It is further illustrated in Fig. 1 that our unsupervised

*Electronic address: ypan@zju.edu.cn

†Electronic address: Guofeng.Zhang@polyu.edu.hk

‡Electronic address: shuming_cheng@tongji.edu.cn

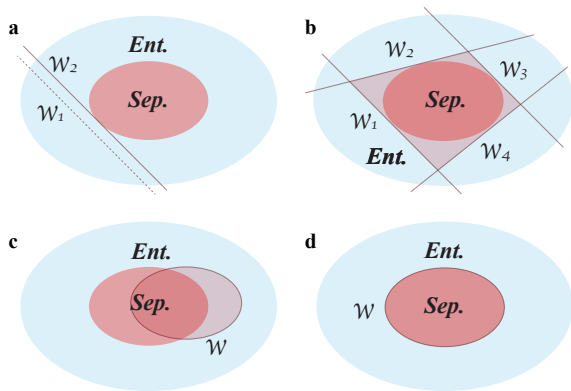


FIG. 1: **The geometrical interpretation of entanglement detection via entanglement witnesses.** (a) Standard linear entanglement witnesses. The witness \mathcal{W}_2 is finer than \mathcal{W}_1 . (b) A proper set of linear entanglement witnesses is able to form a closed area which encloses all separable states. Here $\mathcal{W}_1, \dots, \mathcal{W}_4$ are used as examples. (c) An imperfect nonlinear entanglement witness could be generated via supervised learning method if we cannot label enough samples to cover the space of entangled states. (d) A near-perfect nonlinear witness \mathcal{W} can be approximately constructed by the unsupervised neural network if the generated training data span the space of separable states.

neural nets are essentially trained to search for proper nonlinear entanglement witnesses which near-perfectly construct the boundary between separable and entangled samples. Numerical results show that it is able to achieve extremely high accuracy of entanglement detection with above 97.5% on average, and even capable to detect partial entanglement within subsystems, e.g., bi-separable states in 3-qubit system with accuracy above 97.7%.

II. UNSUPERVISED ENTANGLEMENT DETECTION

A. The task of detecting entanglement

Entanglement is not only of significant importance to understand quantum theory at the fundamental level [1], but also has found applications in information protocols, such as quantum teleportation [?]. For a given n -partite quantum system, entanglement associated with the state is defined in a passive way in which a state ρ is entangled if and only if it cannot be described in a fully-separable form of [?]

$$\rho_{\text{sep}} = \sum_{i=1}^m \lambda_i \rho_i^1 \otimes \dots \otimes \rho_i^j \otimes \dots \otimes \rho_i^n \quad (1)$$

with non-negative coefficients satisfying $\sum_{i=1}^m \lambda_i = 1$. Here ρ_i^j denotes the state density matrix of the j -th subsystem. Obviously, all of the separable states as per (1) form a convex set in the sense that any convex combination of these states in this set also belong to the same

state set. It is noted that the above definition of entanglement does not fully capture the entangled structure in the state, e.g., the partial entanglement [?], which will be discussed in the later section.

In practice, whether a given state ρ is entangled or not can be determined via an entanglement witness [1, 10]. Indeed, as shown in Fig. 1a, an entanglement witness essentially defines a hyperplane which separates the entangled state from the convex set of separable states. Furthermore, it has been shown in [1] that it is impossible for one linear witness to detect all entangled states, implying that a large set of linear witnesses illustrated in Fig. 1b (could be impractical) or certain nonlinear witness shown in Fig. 1d may be required. Besides, it becomes extremely inefficient and impractical to construct a proper witness for an arbitrary state, especially in high-dimensional systems. In the following, we propose a complex-valued neural network trained in unsupervised manner to search for the nonlinear entanglement witnesses as desired.

B. Constructing the complex-valued neural networks

As shown in Fig. 2, our networks could be decomposed into two parts: One is the pseudo-siamese neural network (in the red dashed box) and the other is the GAN (in the purple dashed box). The complex-valued neural network receives the density state matrix as the input. The building modules for these networks are detailed in Appendix A.

The pseudo-siamese neural network consists of two encoders sharing the same network structure, labelled as \mathcal{E}_r and \mathcal{E}_g , respectively. In contrast to the original siamese network [27] which requires quadratic pairs as input, the pseudo-siamese network only requires a single input ρ_{real} be fed to the first encoder \mathcal{E}_r . The second input ρ_{gen} to the second encoder \mathcal{E}_g is automatically generated by the decoder \mathcal{G} whose aim is to reconstruct ρ_{real} . Therefore, the pseudo-siamese network trains much faster than the original siamese network while inherits its few-shot learning ability. In principle, these two encoders competes with each other to produce a pair of indistinguishable feature vectors \mathbf{v}_1 and \mathbf{v}_2 . The performance is evaluated by the cost function

$$\begin{aligned} \mathcal{L}_1 &= \mathbb{E}_{\rho_{\text{real}}} \|\mathcal{E}_r(\rho_{\text{real}}) - \mathcal{E}_g(\mathcal{G}(\mathcal{E}_r(\rho_{\text{real}})))\| \\ &= \mathbb{E}_{\rho_{\text{real}}} \|\mathbf{v}_1 - \mathbf{v}_2\|, \end{aligned} \quad (2)$$

where the norm $\|\mathbf{x}\|$ could be the L_p -norm of any complex vector \mathbf{x} with $\|\mathbf{x}\|_p \equiv (|\Re(\mathbf{x})|^p + |\Im(\mathbf{x})|^p)^{1/p}$. Here 2-norm is chosen for Eq. (2). As the two inputs to the encoders \mathcal{E}_r and \mathcal{E}_g are slightly different, the two encoders would not share the same weight parameters after training [28].

Combining the encoder \mathcal{E}_r with \mathcal{G} yields an encoder-decoder structure which aims to produce fake samples

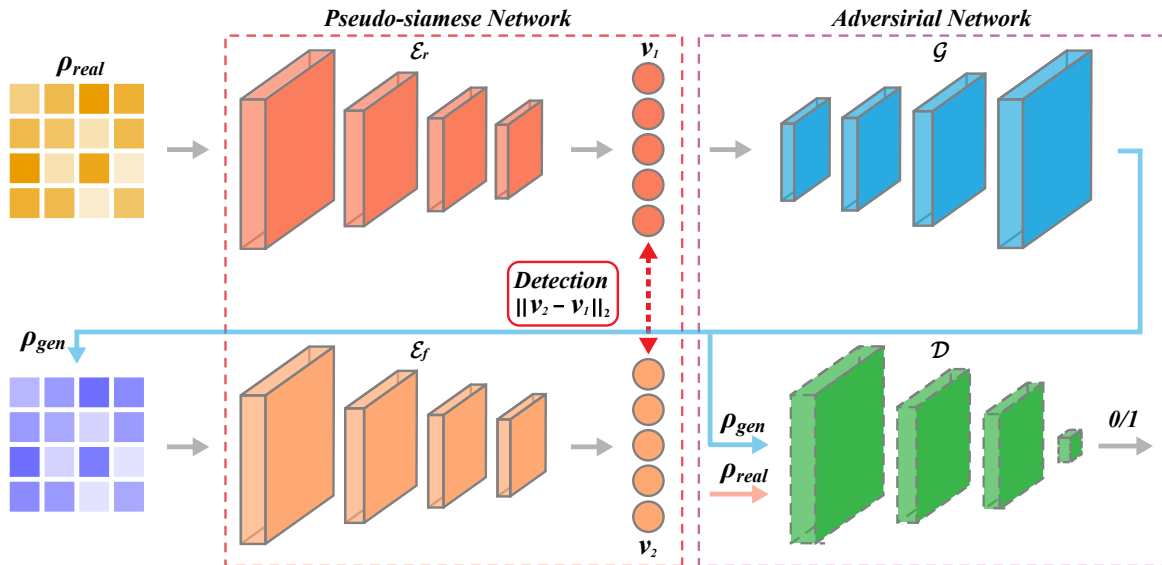


FIG. 2: **Structure of the complex-valued neural network.** The complex-valued network is composed of two parts: One is the pseudo-siamese network in the red dashed box and the other is a GAN in the purple dashed box. The pseudo-siamese neural network consists of two encoders \mathcal{E}_r and \mathcal{E}_g that share the same network structure. ρ_{gen} is generated by \mathcal{G} . The discriminator network \mathcal{D} is a binary classifier which outputs either 0 or 1. The generator \mathcal{G} and discriminator \mathcal{D} form the GAN, which aims to produce a ρ_{gen} that is as close as possible to ρ_{real} .

that are close to real ones. Thus we introduce the loss function

$$\mathcal{L}_2 = \mathbb{E}_{\rho_{\text{real}}} \|\rho_{\text{real}} - \mathcal{G}(\mathcal{E}_r(\rho_{\text{real}}))\| = \mathbb{E}_{\rho_{\text{real}}} \|\rho_{\text{real}} - \rho_{\text{gen}}\| \quad (3)$$

to quantify its performance. In analogy to classical autoencoders [29], it is found that L_1 -norm achieves better performance than that of $p = 2$ for this loss term.

An optional discriminator network could be introduced for additional adversarial training. The discriminator \mathcal{D} and generator \mathcal{G} form the GAN (Fig. 2) which could enhance the ability of \mathcal{G} to produce more realistic quantum samples. Indeed, \mathcal{D} is a binary classifier trained to discriminate fake samples from real ones. The two cost functions for this adversarial net are given by

$$\mathcal{L}_{\text{adv1}} = \mathbb{E}_{\rho_{\text{real}}} (-\mathcal{D}(\rho_{\text{real}}) + \mathcal{D}(\mathcal{G}(\mathcal{E}_r(\rho_{\text{real}})))), \quad (4)$$

$$\mathcal{L}_{\text{adv2}} = \mathbb{E}_{\rho_{\text{real}}} (-\mathcal{D}(\mathcal{G}(\mathcal{E}_r(\rho_{\text{real}})))), \quad (5)$$

which are alternatively minimized via gradient descent method. Specifically, the gradients are clipped between -1 and 1 , turning the network into a Wasserstein GAN which is easy to train [30]. In each round, the parameters of \mathcal{D} are updated by minimizing $\mathcal{L}_{\text{adv1}}$, while the parameters of \mathcal{G} and \mathcal{E}_r are updated by minimizing $\mathcal{L}_{\text{adv2}}$.

Finally, by combining (2)-(5), the complex-valued neural network is trained by alternatively minimizing $\mathcal{L}_{\text{adv1}}$ and

$$\mathcal{L}_3 = w_1 \cdot \mathcal{L}_1 + w_2 \cdot \mathcal{L}_2 + w_a \cdot \mathcal{L}_{\text{adv2}}, \quad (6)$$

with the weight parameters w_1 , w_2 , and w_a being chosen adaptively.

C. Training the networks via unsupervised learning

If the complex-valued network is trained with separable states only, an entangled state would result in a feature vector v_{ent} distinct from that of the generated one in the latent space. Indeed, the entire training and prediction process can be divided into three steps as follows.

- 1) Preparing separable states as training samples. Following Eq. (1), each ρ_i^j is generated via $HH^\dagger / (\text{Tr}[HH^\dagger])$, where H is a complex-valued matrix whose real and imaginary parts of each entry are sampled from independent Gaussian distributions. It is noted that this sampling method could cover the whole space of separable states [31].
- 2) Training the neural network on the generated set of separable states by alternatively minimizing $\mathcal{L}_{\text{adv1}}$ as per Eq.(4) and \mathcal{L}_3 as per Eq. (6) via the gradient descent method.
- 3) Determining the decision threshold value b on the test set after training. We choose b to satisfy

$$\frac{\text{FN}}{\text{TP} + \text{FN}} = \frac{\text{FP}}{\text{FP} + \text{TN}}, \quad (7)$$

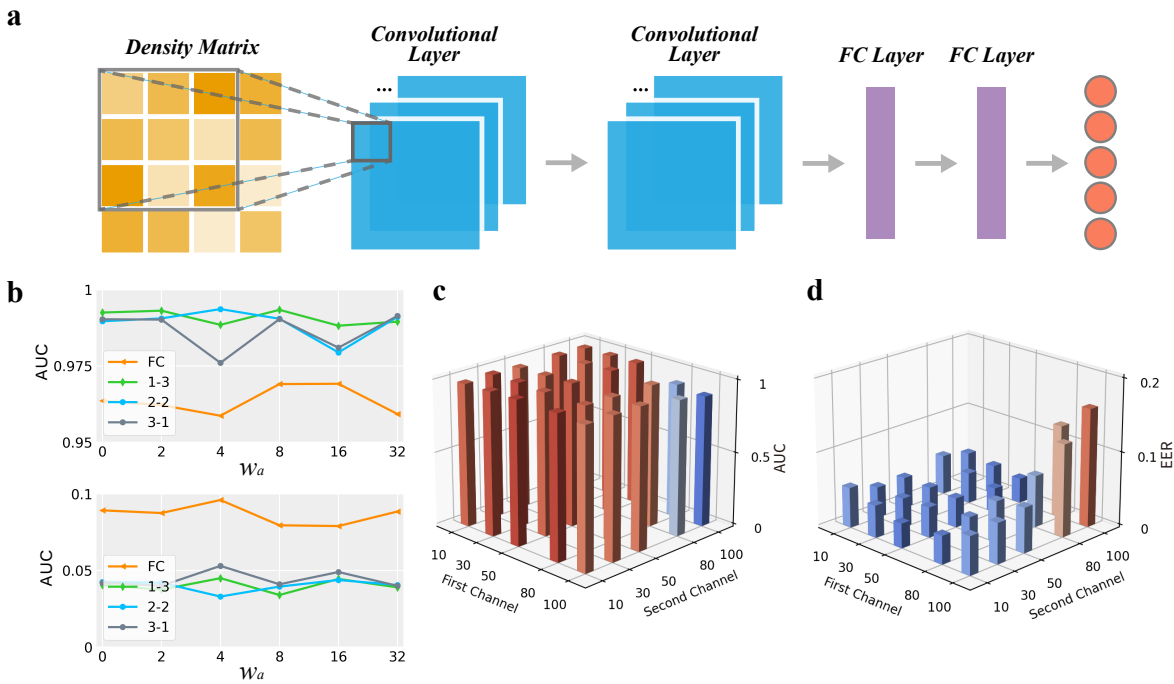


FIG. 3: **Detection of 2-qubit states.** (a) 4-layer neural network structure of the encoder, including two convolutional layers followed by two FC layers. The structures of the encoder and decoder are symmetric. The structure of the discriminator is the same as the encoder, with an additional normalization layer to produce a scalar output. (b) The performance of the neural networks with the first two layers being convolutional or FC. The convolutional kernel size combinations that have been tested are 1×1 and 3×3 , 2×2 and 2×2 , 3×3 and 1×1 , with the number of output channels being 10 and 30, respectively. If the first two layers are FC, the number of output channels is set to 32 and 128, respectively. (e-f) AUCs and EERs with different number of output channels for convolutional layers. The convolutional kernel sizes are 2×2 and 2×2 .

where TP, FP, TN, and FN refer to the number counts of true positive, false positive, true negative, and false negative samples. Here, being positive or negative stands for a separable or entangled sample. Choosing b to satisfy (7) implies that the probabilities of misclassifying entangled and separable states are the same on the test set. Hence, if the score of a quantum state is larger than this b , then it will be detected as entangled.

For each ρ in the test set, its score for entanglement detection can be defined as

$$\mathcal{A}(\rho) = \|\mathcal{E}_r(\rho) - \mathcal{E}_g(\mathcal{G}(\mathcal{E}_r(\rho)))\|_2. \quad (8)$$

It could be further expressed in a witness-like form of

$$\mathcal{A}(\rho) = \|(\mathcal{W}_{\mathcal{E}_g} \mathcal{W}_{\mathcal{G}} - \mathcal{I}) \mathcal{W}_{\mathcal{E}_r} \cdot \text{vec}(\rho)\|_2 = \|\mathcal{W} \cdot \text{vec}(\rho)\|_2, \quad (9)$$

where $\mathcal{W}_{\mathcal{E}_f(\mathcal{G})}$ denotes the weight tensor which generates the corresponding linear and nonlinear network transformations. For this reason, the neural network model can be regarded as trying to determine the nonlinear witness \mathcal{W} which approximately characterizes the boundary between separable and entangled states, without relying on samples of entangled states during training.

Alternately, there is another way to implement the model for prediction without the test dataset, making

both training and prediction independent of any information of entangled states. This is achieved by determining b as

$$b = \max_{\rho_{\text{sep}}} \mathcal{A}(\rho). \quad (10)$$

Obviously, this approach leads to a higher detection accuracy than using Eq. (7). Since both the training and implementation do not rely on entangled samples, this approach is computationally efficient. More importantly, the major advantage of our unsupervised learning framework lies in its scalability, as generating sufficient entangled states for training becomes impractical for high-dimensional quantum systems.

III. NUMERICAL RESULTS

A. Detecting 2-qubit entangled states

The number of training samples for 2-qubit case is 160000, all composed of separable states. The number of testing samples is 80000, including 40000 separable states and 40000 entangled states. 2-qubit separable states are

generated by

$$\rho_{\text{sep}} = \sum_{i=1}^m \lambda_i \rho_i^1 \otimes \rho_i^2, \quad (11)$$

where $\sum_{i=1}^m \lambda_i = 1$ and $0 \leq \lambda_i \leq 1$, with m iterating from 1 to 20. Entangled states are selected from randomly generated states of the entire system using PPT criterion.

We use two evaluation metrics for binary classification. The first metric is the Area Under Curve (AUC) of the Receiver Operating Characteristic (ROC) curve, which is created by plotting the True Positive Rate ($\text{TPR} = \text{TP}/(\text{TP} + \text{FN})$) against the False Positive Rate ($\text{FPR} = \text{FP}/(\text{FP} + \text{TN})$) using the similarity score defined in (8) for various values of b [32]. The second metric is Equal Error Rate (EER), which is defined as $\text{FN}/(\text{TP} + \text{FN})$ when (7) holds [33]. The structure of the 4-layer encoder is illustrated in Fig. 3a. The last two layers of the encoder are Fully-Connected (FC) layers, with output channels being 64 and 10, respectively. The first two layers can be convolutional with different kernels and different number of output channels, or fully connected as tested in Fig. 3b. The best performance of the model has been achieved with the convolutional kernel size of the first two layers being 2×2 and 2×2 . The best AUC is 0.99 and EER is 2.99%, attained at a small w_a which is the weight of adversarial cost for training. As shown in Fig. 3b, convolutional layer performs much better than FC layer, with AUC being consistently higher than 0.975 and EER lower than 5%. Fig. 3e-f shows the performance of convolutional neural networks when the number of output channels varies, indicating that a small number of output channels is enough to extract the features of entanglement for 2-qubit states.

B. Detecting 3-qubit entangled states

An entangled 3-qubit state can be classified into several types, e.g. bi-separable states and bound entangled states [24]. The 3-qubit state is fully-separable if

$$\rho_{\text{sep}} = \sum_{i=1}^m \lambda_i \rho_i^1 \otimes \rho_i^2 \otimes \rho_i^3. \quad (12)$$

The distribution of 3-qubit states is illustrated in Fig. 4a. In this case, successful supervised learning requires that one can generate enough and balanced samples for all types of entanglement, which cannot be guaranteed by the current random sampling techniques. In contrast, a universal entanglement detector could be built using only the fully-separable samples if unsupervised learning method is employed.

The numerical results in Fig. 4b are based on a dataset consisting of 160000 training samples and 200000 test samples. The training samples are fully-separable states, and the test samples include 40000 fully-separable states,

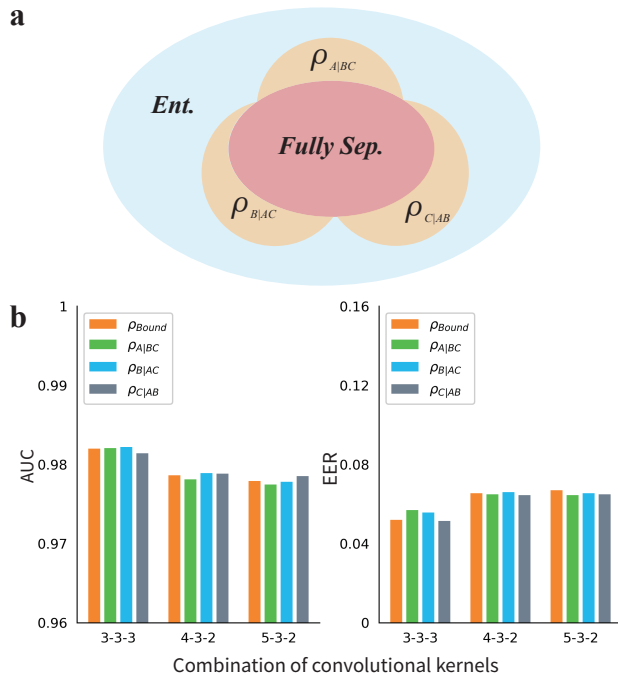


FIG. 4: **Detection of 3-qubit states.** (a) Distribution of 3-qubit states. $\rho_{A|BC}$ is a bi-separable state with qubit B and C entangled. (b) EERs and AUCs with different combinations of convolutional kernels, where $i-j-k$ stands for the kernel sizes of the three convolutional layers.

40000 bound entangled states and 120000 bi-separable states (40000 for each subtype). To accommodate the 8×8 density matrix input, a third convolutional layer is added. The number of the output channels for the three convolution layers is 10, 30, 50, respectively. Since the unsupervised model focuses on detecting the feature of separability instead of the features of different types of entanglement, it has achieved similar detection accuracy on four types of entangled samples.

C. Scalability up to 10-qubit states

The unsupervised learning method is applied on 5- and 10-qubit states to study its scalability. Without loss of generality, we focus on the classification of pure states for which geometrical entanglement measure can be computed [34]. Note that the geometrical measure is only used to label the entangled states for the test dataset. The separable pure states are generated by

$$|\psi_{\text{sep}}\rangle = \sum_{i=1}^m \lambda_i |\psi_i^1\rangle \cdots \otimes |\psi_i^j\rangle \otimes \cdots \otimes |\psi_i^n\rangle, \quad (13)$$

where $|\psi_i^j\rangle$ is a randomly generated pure state vector of the j -th qubit. The real and imaginary parts of the complex-valued vector are sampled from an independent Gaussian distribution. The density matrix

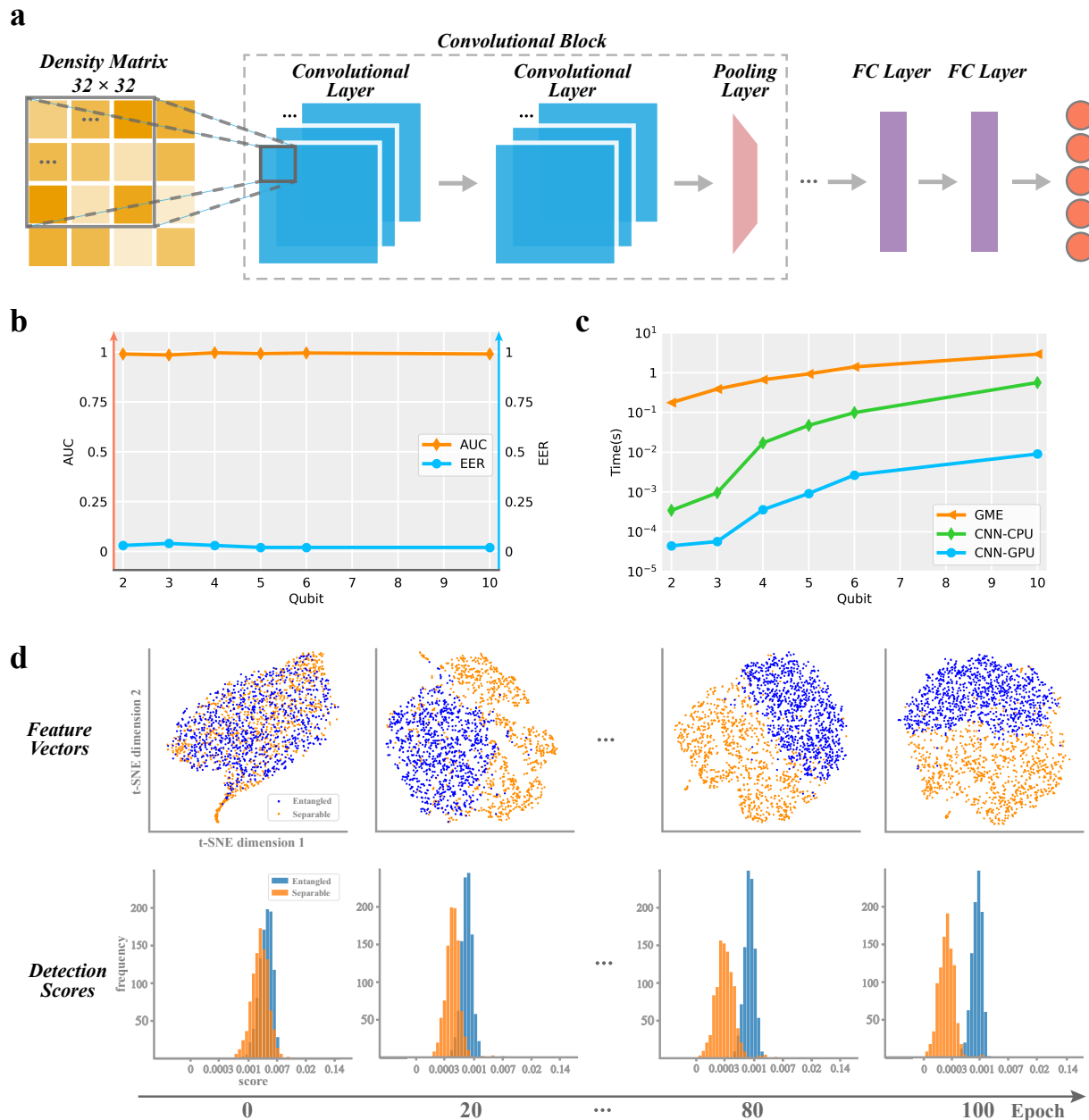


FIG. 5: **Scalability of unsupervised learning.** (a) The neural network structure of the encoder for 5-qubit pure states. The convolutional block is composed of two convolutional layers and a 2×2 max pooling layer. (b) AUCs and EERs achieved by the unsupervised learning method as the number of qubits increases. (c) The comparison of inference time between the up-to-date numerical method for computing the Geometrical Entanglement Measure (GME) and the neural network method. (d) The evolution of feature vectors and detection scores for 1000 separable and 1000 entangled samples of 5-qubit states during training.

$\rho_{\text{sep}} = |\psi_{\text{sep}}\rangle\langle\psi_{\text{sep}}|$ is used as the input to the neural network. Fig. 5a depicts the network structure of the encoder for entanglement detection in 5-qubit states, where a max pooling layer has been added to handle the increased dimension of the input. For 10-qubit states, we adopt three convolutional layers and increase the max pooling size to 4×4 . The training dataset is composed of

160000 separable states, and the test dataset is composed of 40000 separable and 40000 entangled states. The entangled states are found by randomly generating 5- and 10-qubit pure states and computing their entanglement measures using the numerical method from [34]. See Appendix B for the details of the algorithm.

As shown in Fig. 5b, the unsupervised model achieves

an AUC of 0.9952 and an EER of 2.02% for entanglement detection in 10-qubit states. The EER is 0.54% for entanglement detection in 5-qubit states, which means only 54 in 10000 states are misclassified. The short inference time is another advantage of the neural network model. The inference time of the neural network model on GPU is about tens of microseconds to hundreds of microseconds for up to 10 qubits (Fig. 5c), which is significantly faster than the up-to-date numerical method which takes the state vector instead of density matrix as the input for computing the geometrical entanglement measure.

The upper half of Fig 5d shows the evolution of feature vectors of 1000 separable and 1000 entangled states in the training process for 5-qubit states. We visualize the evolution by t-SNE method [35] which maps the feature vectors to two-dimensional space. In the first 10 epochs, the entangled and separable states are mixed up in the latent space and difficult to distinguish. After 20 epochs, the feature vectors start to split into two set. In the last 20 epochs, the feature vectors of separable states are separated completely from the feature vectors of entangled states, with very few exceptions. A similar evolution can be seen in the distribution of detection scores of the input states. After training, the detection scores of separable states are more closed to zero, while the scores of entangled states are concentrated around 0.001.

IV. CONCLUSIONS AND DISCUSSIONS

We have proposed an efficient and scalable method with unsupervised learning to detect quantum entan-

glement. Specifically, we build up a class of complex-valued pseudo-siamese neural networks which is easy to implement as it is trained without entangled samples. Moreover, it is scalable to detect entanglement of high-dimensional systems where sufficient labelled entangled samples become difficult to obtain, and our numerical analysis finds that we could still obtain a rather high accuracy with above 97.5% on average for multi-qubit system from 2-qubit to 10-qubit. For this reason, we believe that our work provides a promising tool to detect quantum features of high-dimensional quantum data.

Finally, it is noted that we exploit the convexity of separable samples and thus reformulate entanglement detection as an anomaly detection problem, for which the unsupervised neural networks are suitable. Since other useful quantum features, such as Bell nonlocality and Einstein-Podolsky-Rosen steerability, also share the same property that it is defined as a distinguishable sample from a convex set, it is evident that our work can be readily generalized to solve the similar detection problem.

Acknowledgements

This research was supported by the National Natural Science Foundation of China under Grants No. 61703364 and No. 62088101. G. F. also acknowledges support from Hong Kong Research Grant Council (Grants No. 15208418 and No. 15203619) and Shenzhen Fundamental Research Fund, China (Grant No. JCYJ20190813165207290).

-
- [1] Ryszard Horodecki, Paweł Horodecki, Michał Horodecki, and Karol Horodecki. Quantum entanglement. *Reviews of modern physics*, 81(2):865, 2009.
 - [2] Alexander Streltsov, Gerardo Adesso, and Martin B. Plenio. Colloquium: Quantum coherence as a resource. *Rev. Mod. Phys.*, 89:041003, Oct 2017. doi: 10.1103/RevModPhys.89.041003. URL <https://link.aps.org/doi/10.1103/RevModPhys.89.041003>.
 - [3] Eric Chitambar and Gilad Gour. Quantum resource theories. *Rev. Mod. Phys.*, 91:025001, Apr 2019. doi: 10.1103/RevModPhys.91.025001. URL <https://link.aps.org/doi/10.1103/RevModPhys.91.025001>.
 - [4] Michael A. Nielsen and Isaac I. Chuang. *Quantum computation and quantum information*. Cambridge University Press, Cambridge, 2000.
 - [5] Ivan H. Deutsch. Harnessing the power of the second quantum revolution. *PRX Quantum*.
 - [6] Asher Peres. Separability criterion for density matrices. *Physical Review Letters*, 77(8):1413, 1996.
 - [7] Leonid Gurvits. Classical deterministic complexity of edmonds' problem and quantum entanglement. In *Proceedings of the thirty-fifth annual ACM symposium on Theory of computing*, pages 10–19, 2003.
 - [8] Ryszard Horodecki, Michał Horodecki, and Paweł Horodecki. Teleportation, bell's inequalities and inseparability. *Physics Letters A*, 222(1-2):21–25, 1996.
 - [9] Barbara M Terhal. Bell inequalities and the separability criterion. *Physics Letters A*, 271(5-6):319–326, 2000.
 - [10] Otfried Gühne and Géza Tóth. Entanglement detection. *Physics Reports*, 474(1-6):1–75, 2009.
 - [11] Jacob Biamonte, Peter Wittek, Nicola Pancotti, Patrick Rebentrost, Nathan Wiebe, and Seth Lloyd. Quantum machine learning. *Nature*, 549(7671):195–202, 2017.
 - [12] Jing Xiao, YuPing Yan, Jun Zhang, and Yong Tang. A quantum-inspired genetic algorithm for k-means clustering. *Expert Systems with Applications*, 37(7):4966–4973, 2010.
 - [13] Seth Lloyd, Masoud Mohseni, and Patrick Rebentrost. Quantum principal component analysis. *Nature Physics*, 10(9):631–633, 2014.
 - [14] Ewin Tang. A quantum-inspired classical algorithm for recommendation systems. In *Proceedings of the 51st Annual ACM SIGACT Symposium on Theory of Computing*, pages 217–228, 2019.
 - [15] Marin Bukov, Alexandre GR Day, Dries Sels, Phillip Weinberg, Anatoli Polkovnikov, and Pankaj Mehta. Re-

- inforcement learning in different phases of quantum control. *Physical Review X*, 8(3):031086, 2018.
- [16] Robert J Chapman, Christopher Ferrie, and Alberto Peruzzo. Experimental demonstration of self-guided quantum tomography. *Physical review letters*, 117(4):040402, 2016.
- [17] Easwar Magesan, Jay M Gambetta, Antonio D Córcoles, and Jerry M Chow. Machine learning for discriminating quantum measurement trajectories and improving read-out. *Physical review letters*, 114(20):200501, 2015.
- [18] Alexander Hentschel and Barry C Sanders. Machine learning for precise quantum measurement. *Physical review letters*, 104(6):063603, 2010.
- [19] Giuseppe Carleo and Matthias Troyer. Solving the quantum many-body problem with artificial neural networks. *Science*, 355(6325):602–606, 2017.
- [20] Li Huang and Lei Wang. Accelerated monte carlo simulations with restricted boltzmann machines. *Physical Review B*, 95(3):035105, 2017.
- [21] Juan Carrasquilla and Roger G Melko. Machine learning phases of matter. *Nature Physics*, 13(5):431–434, 2017.
- [22] Sirui Lu, Shilin Huang, Keren Li, Jun Li, Jianxin Chen, Dawei Lu, Zhengfeng Ji, Yi Shen, Duanlu Zhou, and Bei Zeng. Separability-entanglement classifier via machine learning. *Physical Review A*, 98(1):012315, 2018.
- [23] Mu Yang, Chang-liang Ren, Yue-chi Ma, Ya Xiao, Xiang-Jun Ye, Lu-Lu Song, Jin-Shi Xu, Man-Hong Yung, Chuan-Feng Li, and Guang-Can Guo. Experimental simultaneous learning of multiple nonclassical correlations. *Physical review letters*, 123(19):190401, 2019.
- [24] Yue-Chi Ma and Man-Hong Yung. Transforming bell’s inequalities into state classifiers with machine learning. *npj Quantum Information*, 4(1):1–10, 2018.
- [25] Nana Liu and Patrick Rebentrost. Quantum machine learning for quantum anomaly detection. *Phys. Rev. A*, 97:042315, Apr 2018. doi: 10.1103/PhysRevA.97.042315. URL <https://link.aps.org/doi/10.1103/PhysRevA.97.042315>.
- [26] Jin-Min Liang, Shu-Qian Shen, Ming Li, and Lei Li. Quantum anomaly detection with density estimation and multivariate gaussian distribution. *Phys. Rev. A*, 99:052310, May 2019. doi: 10.1103/PhysRevA.99.052310. URL <https://link.aps.org/doi/10.1103/PhysRevA.99.052310>.
- [27] Gregory Koch, Richard Zemel, and Ruslan Salakhutdinov. Siamese neural networks for one-shot image recognition. In *ICML deep learning workshop*, volume 2. Lille, 2015.
- [28] Lloyd H Hughes, Michael Schmitt, Lichao Mou, Yuanyuan Wang, and Xiao Xiang Zhu. Identifying corresponding patches in sar and optical images with a pseudo-siamese cnn. *IEEE Geoscience and Remote Sensing Letters*, 15(5):784–788, 2018.
- [29] Phillip Isola, Jun-Yan Zhu, Tinghui Zhou, and Alexei A Efros. Image-to-image translation with conditional adversarial networks. In *Proceedings of the IEEE conference on computer vision and pattern recognition*, pages 1125–1134, 2017.
- [30] Martin Arjovsky, Soumith Chintala, and Léon Bottou. Wasserstein generative adversarial networks. In *International conference on machine learning*, pages 214–223, 2017.
- [31] Karol Zyczkowski and Hans-Jürgen Sommers. Induced measures in the space of mixed quantum states. *Journal of Physics A: Mathematical and General*, 34(35):7111, 2001.
- [32] Christopher D Brown and Herbert T Davis. Receiver operating characteristics curves and related decision measures: A tutorial. *Chemometrics and Intelligent Laboratory Systems*, 80(1):24–38, 2006.
- [33] Xiao-Hua Zhou, Donna K McClish, and Nancy A Obuchowski. *Statistical methods in diagnostic medicine*, volume 569. John Wiley & Sons, 2009.
- [34] Mengshi Zhang, Guyan Ni, and Guofeng Zhang. Iterative methods for computing u-eigenvalues of non-symmetric complex tensors with application in quantum entanglement. *Computational Optimization and Applications*, 75(3):779–798, 2020.
- [35] Laurens van der Maaten and Geoffrey Hinton. Visualizing data using t-sne. *Journal of machine learning research*, 9(Nov):2579–2605, 2008.
- [36] Chiheb Trabelsi, Olexa Bilaniuk, Ying Zhang, Dmitry Serdyuk, Sandeep Subramanian, Joao Felipe Santos, Soroush Mehri, Negar Rostamzadeh, Yoshua Bengio, and Christopher J Pal. Deep complex networks. In *International Conference on Learning Representations*, 2018.
- [37] Adam Paszke, Sam Gross, Soumith Chintala, Gregory Chanan, Edward Yang, Zachary DeVito, Zeming Lin, Alban Desmaison, Luca Antiga, and Adam Lerer. Automatic differentiation in pytorch. 2017.

Appendix A: Complex-valued neural network

We build the complex-valued neural network based on the work of Trabelsi et al. [36]. The codes are available at https://github.com/ewellchen/Entanglement_detection. The two-dimensional convolutional (denoted as $*$) and fully-connected (denoted as \cdot) operations of the weight w and input z in the complex domain are defined by

$$\begin{aligned} w * z &= \Re\{w\} * \Re\{z\} - \Im\{w\} * \Im\{z\} \\ &\quad + i(\Im\{w\} * \Re\{z\} + \Re\{w\} * \Im\{z\}), \\ w \cdot z &= \Re\{w\}\Re\{z\} - \Im\{w\}\Im\{z\} \\ &\quad + i(\Re\{w\}\Im\{z\} + \Im\{w\}\Re\{z\}), \end{aligned} \quad (\text{A1})$$

where \Re and \Im represent the real and imaginary part of the vector or matrix, respectively. The formulation of the Complex-valued Rectified Linear Unit (CReLU) is given by

$$\text{CReLU}(z) = \text{ReLU}(\Re(z)) + i\text{ReLU}(\Im(z)), \quad (\text{A2})$$

which introduces nonlinearity into the network transformation. The Batch Normalization (BN) layer is implemented by multiplying the 0-centered data ($z - \mathbb{E}[z]$) with the inverse square root of the covariance as

$$\begin{aligned} \mathcal{V} &= \begin{pmatrix} \text{Cov}(\Re\{z\}, \Re\{z\}) & \text{Cov}(\Re\{z\}, \Im\{z\}) \\ \text{Cov}(\Im\{z\}, \Re\{z\}) & \text{Cov}(\Im\{z\}, \Im\{z\}) \end{pmatrix}, \\ \tilde{z} &= (\mathcal{V})^{-\frac{1}{2}}(z - \mathbb{E}[z]), \\ \text{BN}(\tilde{z}) &= \begin{pmatrix} \gamma_{rr} & \gamma_{ri} \\ \gamma_{ri} & \gamma_{ii} \end{pmatrix} \tilde{z} + \beta. \end{aligned} \quad (\text{A3})$$

The parameters $\gamma_{r(i)r(i)}$ and β are trainable. Each convolutional layer is composed of a convolutional operation, a CReLU and a BN layer. The first fully-connected layer is composed of a fully-connected operation and a CReLU. The last fully-connected layer generates the final output directly via a fully-connected operation. The operations defined above are differentiable, which means the neural network could be trained efficiently with back-propagation. The gradient is calculated with respect to the real-valued cost function \mathcal{L} as

$$\nabla_{\mathcal{L}}(z) = \frac{\partial \mathcal{L}}{\partial z} = \frac{\partial \mathcal{L}}{\partial z_r} + i \frac{\partial \mathcal{L}}{\partial z_i} = \Re(\nabla_{\mathcal{L}}(z)) + i \Im(\nabla_{\mathcal{L}}(z)). \quad (\text{A4})$$

The back-propagation updates the complex-valued parameter $t = t_r + it_i$ of the neural network by

$$\begin{aligned} \nabla_{\mathcal{L}}(t) &= \frac{\partial \mathcal{L}}{\partial t} = \frac{\partial \mathcal{L}}{\partial t_r} + i \frac{\partial \mathcal{L}}{\partial t_i} \\ &= \frac{\partial \mathcal{L}}{\partial z_r} \frac{\partial z_r}{\partial t_r} + \frac{\partial \mathcal{L}}{\partial z_i} \frac{\partial z_i}{\partial t_r} + i \left(\frac{\partial \mathcal{L}}{\partial z_r} \frac{\partial z_r}{\partial t_i} + \frac{\partial \mathcal{L}}{\partial z_i} \frac{\partial z_i}{\partial t_i} \right) \\ &= \frac{\partial \mathcal{L}}{\partial z_r} \left(\frac{\partial z_r}{\partial t_r} + i \frac{\partial z_r}{\partial t_i} \right) + \frac{\partial \mathcal{L}}{\partial z_i} \left(\frac{\partial z_i}{\partial t_r} + i \frac{\partial z_i}{\partial t_i} \right) \\ &= \Re(\nabla_{\mathcal{L}}(z)) \left(\frac{\partial z_r}{\partial t_r} + i \frac{\partial z_r}{\partial t_i} \right) \\ &\quad + \Im(\nabla_{\mathcal{L}}(z)) \left(\frac{\partial z_i}{\partial t_r} + i \frac{\partial z_i}{\partial t_i} \right), \end{aligned} \quad (\text{A5})$$

which could be implemented using Pytorch [37].

Appendix B: Computing the GME of quantum pure states

We employ the algorithm proposed in [34] to compute the GME for an arbitrary quantum pure state. The al-

gorithm is based on a tensor version of the Gauss-Seidel method for computing unitary eigenpairs (U-eigenpairs) of a non-symmetric complex tensor \mathcal{A} which corresponds to the given quantum pure state.

Algorithm 1 [34] *Computing the U-eigenpairs of an $n_1 \times \dots \times n_m$ non-symmetric complex tensor \mathcal{A} .*

Step 1 (Initial step): Let $\mathcal{S} = \text{sym}(\mathcal{A})$ be the symmetric embedding of \mathcal{A} , and $n = n_1 + \dots + n_m$. Choose a starting point $\mathbf{x}_0 \in \mathbb{C}^n$ with $\|\mathbf{x}_0\| = 1$, and $0 < \alpha_{\mathcal{S}} \in \mathbb{R}$. Let $\lambda_0 = \mathcal{S}^* \mathbf{x}_0^m$.

Step 2 (Iterating step):

for $k = 1, 2, \dots$, do

$$\begin{aligned} \hat{\mathbf{x}}_k &= \lambda_{k-1} \mathcal{S} \mathbf{x}_{k-1}^{*m-1} + \alpha_{\mathcal{S}} \mathbf{x}_{k-1}, \\ \mathbf{x}_k &= \hat{\mathbf{x}}_k / \|\hat{\mathbf{x}}_k\|, \\ \lambda_k &= \mathcal{S}^* \mathbf{x}_k^m. \end{aligned}$$

end for.

return:

Unitary symmetric eigenpair (US-pair): $\lambda_{\mathcal{S}} = |\lambda_k|$, and $\mathbf{x} = \left(\frac{\lambda_{\mathcal{S}}}{\lambda_k}\right)^{1/m} \mathbf{x}_k$.
Let $\mathbf{x} = (\mathbf{x}^{(1)\top}, \dots, \mathbf{x}^{(m)\top})^\top$, $\mathbf{x}^{(i)} \in \mathbb{C}^{n_i}$, for all $i = 1 : m$.

U-eigenvalue $\lambda_{\mathcal{A}} = \frac{(\sqrt{m})^m}{m!} \lambda_{\mathcal{S}}$.

U-eigenvector $\{\sqrt{m} \mathbf{x}^{(1)}, \dots, \sqrt{m} \mathbf{x}^{(m)}\}$.